Active Spatiotemporal Control of Arg-Gly-Asp-Containing Tetradecapeptide Organomercaptans on Gold with In−Plane Electrochemical Potential Gradients

Q. Wang and P. W. Bohn*

Department of Chemistry and Frederick Seitz Materials Research Laboratory, University of Illinois at Urbana-Champaign, 600 S. Mathews Avenue, Urbana, Illinois 61801

Received: March 11, 2003; In Final Form: June 12, 2003

Surface immobilized peptides and proteins containing the tripeptide sequence Arg-Gly-Asp (RGD) are of interest because of their ability to bind to members of the integrin superfamily of cell-surface receptors and thereby direct cellular haptotaxis. Two-component counterpropagating gradients of organothiols terminated with an RGD-containing tetradecapeptide and the cell-adhesion-resistant thiol, mercaptoundecanol (MUD), were electrochemically generated by coupling in-plane electrochemical potential gradients with the electrosorption reactions of organothiols to vary the composition laterally. One- and two-component gradients formed from model alkanethiols and peptide-terminated thiols as a function of local composition were probed by spatially resolved electrochemical stripping analysis and Fourier transform infrared external reflection spectroscopy (FTIR-ERS), using the IR spectra to map the local composition and the shift in desorption peak potential, E^0_{des}, to assess the degree of surface heterogeneity. The measured lateral composition profiles, $\Gamma(x)$, are well-described by a linear potential gradient model. However, because the two-component gradients are formed in a two-step process, in which a full monolayer of the first component is desorbed in a spatially dependent manner, there is a lower density of adsorbate molecules remaining in the transition region due to partial desorption of organothiols leading to less organized molecular packing.

Introduction

Cellular adhesion to the extracellular matrix (ECM) influences the shape, growth, motility, and metabolism of cells.[1−3] One goal of research in this laboratory is to control cell migration by manipulating the chemical environment presented by the ECM. Gradients of ligands for cell membrane receptors, such as the integrins, are the directing force in cellular haptotaxis in nature,[4−9] being able to modulate the average speed of cell locomotion, for example.[10−15] Systematic variation of cell-substratum adhesion strength has most commonly been achieved by moderating the surface density of ECM proteins,[14] in which the tripeptide sequence arginine-glycine-aspartic acid (RGD) is a common motif competent to induce recognition of the ECM protein by cell membrane receptors from the integrin superfamily.[16−19] However, much of the previous work on ECM effects has addressed the effect of spatially uniform ligand density distributions of on-cell-substratum interactions. Clearly, the creation and quantitative characterization of nonuniform RGD distributions with controlled characteristics will be key to enhanced understanding of cellular adhesion and motility.

Creating well-defined gradients in surface composition to study cell adhesion and motility has proven to be a substantial experimental challenge.[20] The approach taken here exploits the fact that SAMs formed by the adsorption of alkanethiols on Au are structurally well-defined and allow wide flexibility in attaching and patterning ligands. Several methods have been demonstrated that use SAMs to generate gradients in surface properties, including photoimmobilization of peptides on SAMs[21] and reaction-cross diffusion.[22,23] R-Phycoerythrin gradients have been created using a heterobifunctional photolinking agent by changing the exposure time to laser irradiation,[24] and a microfluidic system has recently been used to generate surface and solution gradients of laminin in order to study neuronal growth.[25,26]

Recently, spatiotemporal control over surface composition has been achieved in our laboratory by coupling dynamically controllable electrochemical potential gradients with electrosorption reactions of organothiols to vary the composition profile of one- or two-component SAMs laterally.[27−31] This development opens the way to control the lateral distribution of interfacial properties by melding compositional tailoring with surface patterning. The advantage of the electrochemical approach is that the positions and widths of the gradients are readily controllable in both space and time, even after initial formation. Gradients in surface potential are formed by the injection of an in-plane current in a thin (5 nm $\leq d \leq$ 80 nm) Au film according to

$$V(x) = V_0 + \int_0^x \frac{i\rho(l)}{A} dl \qquad (1)$$

where $V(x)$ is the local surface potential, V_0 is the offset potential, i is the injected current, A is the cross-sectional area of the Au film, and $\rho(l)$ is the local film resistivity at position l. The position and width of $V(x)$ can be controlled by tuning V_0 and i, respectively. In principle, any electrochemical reaction can be mapped directly onto the surface of the working electrode, because reactions only occur at spatial locations where the local potential is favorable. For example, applying a potential gradient, which spans the reductive desorption and oxidative adsorption potentials of a SAM of a thiol, RSH, results in a surface composition profile, $\Gamma_{RSH}(x)$, which proceeds from bare Au on one end to full coverage of thiol at the other end. This

* To whom correspondence should be addressed. E-mail: bohn@scs.uiuc.edu.

10.1021/jp030329h CCC: $25.00
Published on Web 10/24/2003

strategy creates a composition gradient in one component, the originally adsorbed organothiol RSH. Then immersing the one-component gradient in a solution containing a second thiol, R′SH, results in adsorption of R′SH on the exposed bare Au area to form a two-component gradient which contains primarily RSH at one end, R′SH at the other, and counterpropagating gradient concentrations, $\Gamma_{R'SH}(x) = 1 - \Gamma_{RSH}(x)$, of the two components in the intermediate areas. Changing the terminal group, therefore, allows fabrication of two-component systems with spatially graded chemical and physical properties. The placement of the transition region between the two components is dependent on the value of desorption peak potential, E^0_{des}, for the first thiol, RSH.

To better understand what factors affect the range and spatial dispersion properties of achievable composition distributions, it is important to characterize the spatial variation of chemical and physical properties in the transition region. Contact angle measurement and sulface plasmon reflectometry imaging have been used to map the wettability and resonance variation of alkanethiol gradients.[27,28] Adhesion force images of alkanethiol hexadecanethiol−3-mercaptopropanoic acid (HDT−MPA) gradients have been acquired by pulsed-forced-mode atomic force microscopy (AFM) with chemically derivatized AFM tips.[30] In addition, aromatic thiols and amine-terminated thiol gradients have been spatially profiled by surface-enhanced Raman spectroscopy and fluorescence microscopy, respectively.[29,31] In all of these investigations both the chemical composition and physical properties varied as predicted by a combination of eq 1 and the Nernst equation.

The present investigation focuses first on characterizing the packing structure variation of alkanethiol gradients, and then developing RGD-containing gradients which are mapped by FTIR-ERS. On the basis of the electrochemical potential gradient formation protocol, one can expect that molecular packing will vary through the transition region. Electrochemical stripping analysis is used to probe the lateral variation of packing structure for both one-component and two-component gradients. Because the reductive desorption stripping peak position, E^0_{des}, of thiol SAMs depends in part on the additive contributions of the chemical interaction of S with Au and chain−chain attractive interactions,[32,33] E^0_{des} can be used to probe the degree of ordering and the variations of molecular packing in electrochemically derived composition gradients. Initially, model two-component gradients composed of a long-chain (hexadecanethiol, HDT, $n = 16$) and short-chain (3-mercaptopropanoic acid, MPA, $n = 3$) SAMs were formed, and E^0_{des} was mapped through the transition region.

To apply the electrochemical potential method to create gradients of molecules which control haptotaxis, it is necessary to understand in detail how composition varies spatially, and especially how the electrochemical and structural properties of the gradient constituents vary laterally. To this end, experiments are reported here which characterize structural order in the gradient transition region by spatially mapping E^0_{des} as a function of position and assess our ability to form two-component gradients of an RGD-containing tetradecapeptide-terminated thiol, **1**, and 11-mercaptoundecanol (MUD), the latter being resistant to protein adsorption.[34−36] FTIR reflection spectroscopy is used to map the variations in composition as a function of position for comparison between the biologically active gradients of **1** and the model gradients characterized electrochemically.

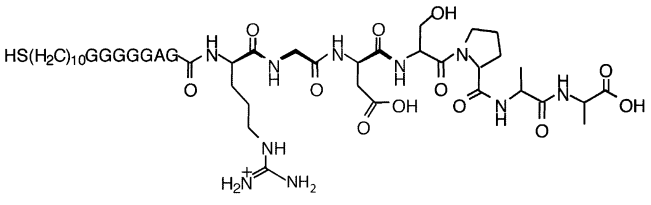

1

Experimental Section

Materials. The RGD-containing thiol, **1**, was synthesized by peptide coupling mercaptoundecanoic acid to the amine terminal of the tetradecapeptide, H_2N-GGGGGAGRGDSPAA-COOH, synthesized at the University of Illinois at Urbana-Champaign Biotechnology Center. The measured molecular mass was 1285.9 Da. 11-Mercaptoundecanol (MUD), hexadecanethiol (HDT), and 3-mercaptopropanoic acid (MPA) were purchased from Aldrich. KOH, Optima grade methanol (MeOH), and 2-propanol were purchased from Fisher Scientific. Absolute ethanol (EtOH) was purchased from Aaper Alcohol and Chemical Company. All reagents were used as received.

Substrate Preparation. Substrates for Au deposition were either glass slides, for FTIR study, or single-polished silicon (100) wafers, for electrochemical stripping analysis of gradients. Prior to metal deposition, slides and wafers were cut into 12 × 50 mm pieces and cleaned in a freshly prepared Piranha solution (4:1 H_2SO_4/H_2O_2. *Caution: Piranha solution is a vigorous oxidant and should be used with extreme caution*.) The slides and wafers were then rinsed thoroughly with double-deionized H_2O and 2-propanol and blown dry with N_2. The samples were then immediately transferred to the evaporation chamber. Chromium (1 nm) was evaporated to promote adhesion of Au on both glass and silicon substrates, followed by evaporation of 50 nm of Au. Samples were stored under N_2 before use.

Gradient Formation. SAMs of **1** and HDT were prepared by immersing Au films in either 20 μM **1** in 1:1 EtOH/H_2O for 24 h or a 1 mM EtOH solution of HDT for 1 h, respectively. A bipotentiostat (Pine Instruments model AFCBPI) employing a Ag/AgCl reference electrode and a Pt mesh counter electrode was used to apply the desired electrochemical potentials to the two ends of the working electrode in deaerated 0.25 M KOH/MeOH. The in-plane electrochemical potential presented by the Au film has been shown previously to be a linear function of position.[29] Typically, SAMs of HDT and **1** were electrolyzed for 1 and 30 min, respectively, to achieve one-component gradients. After electrolysis, the samples were quickly removed from the electrolyte solution, rinsed with MeOH, and reimmersed in a solution of a second thiol (MUD or MPA) for 1 min to form two-component gradients. Gradients composed of **1**/MUD and HDT/MPA were prepared in this manner.

Electrochemical Measurements. Cyclic voltammetry was performed by scanning between 0 and −1.3 V at 100 mV/s vs a Ag/AgCl reference electrode and a Pt mesh counter electrode in 0.25 M KOH/MeOH electrolyte, after purging the cell with Ar for 10 min. For electrochemical stripping analysis of gradients, each gradient sample was diced into 10 pieces, and cyclic voltammetry was performed on each piece.

FTIR External Reflection Spectroscopy. Fourier transform infrared external reflection (FTIR-ERS) spectra were acquired using a Digilab FTS-60A spectrometer (Bio-Rad, Cambridge, MA) equipped with a Harrick Scientific "Seagull" reflection accessory set to 82° and a liquid nitrogen cooled MCT detector and housed in a N_2-purged enclosure. Spectra were acquired from 1024 co-added scans at a resolution of 4 cm^{-1}. All spectra were baseline corrected for accurate comparison. All the electrochemical and FTIR-ERS measurements of gradients were

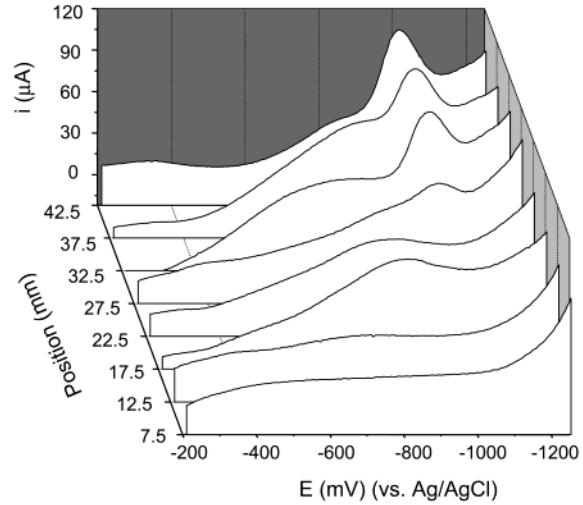

Figure 1. Spatially resolved CVs of a one-component HDT gradient prepared with a 20 mV mm^{-1} in-plane potential gradient in 0.25 M KOH/MeOH. The position labeled 7.5 mm corresponds to an excised sample of the gradient in which the center of the sample was originally 7.5 mm away from the bare Au end.

repeated three times. The results shown here represent one random measurement of the three times.

Results and Discussion

Cyclic Voltammetry of One-Component Gradients. When an alkanethiol SAM on Au is immersed in KOH solution and the potential is swept to the limiting potential imposed by solvent reduction (ca. −1.5 V vs. Ag/AgCl), a reduction peak appears in the range −0.7 to −1.4 V vs Ag/AgCl.[37−39] The peak is assigned to the reductive desorption of the thiolate, $XC_nH_{2n}S^-$

$$AuSC_nH_{2n}X + e^- \rightarrow Au + XC_nH_{2n}S^- \qquad (2)$$

The potential at which this reaction is observed depends on surface coverage and on the degree of ordering in the alkanethiol SAM. The stripping peak position, E^0_{des}, which varies with chain length, *n*, also depends on the strength of the Au−S interaction and chain−chain attractive interactions. Porter et al.[37] have developed an electrical double layer model of alkanethiol SAMs to explain differences in E^0_{des} and found that thinner or less densely packed layers desorb at less negative potentials.

The formation of one-component gradients by applying an in-plane electrochemical potential gradient to an alkanethiol SAM on Au is expected to result in variations of molecular order and packing in the transition region due to the incomplete reductive desorption in this region. Figure 1 shows a series of cyclic voltammograms (CVs) as a function of position along a 50-mm hexadecanethiol (HDT) gradient prepared with a 20 mV mm^{-1} in-plane potential gradient. To acquire spatially resolved CVs the gradient sample was cut into 10 pieces each 5 mm wide, and each piece was studied individually. Each piece was characterized by the spatial position of the center of the piece and by the potential applied to the center position during the original gradient formation process. To avoid edge effects the two end pieces were not measured. Stripping analysis was also employed to characterize other HDT gradients prepared with applied potential windows of different widths, as shown in Figure 2. In all of these experiments the transition region is characterized by fitting the desorption peak potential as a function of spatial position—or equivalently to the potential applied during the stripping phase of the gradient formation protocol, $V(x)$—to a sigmoidal function of the form

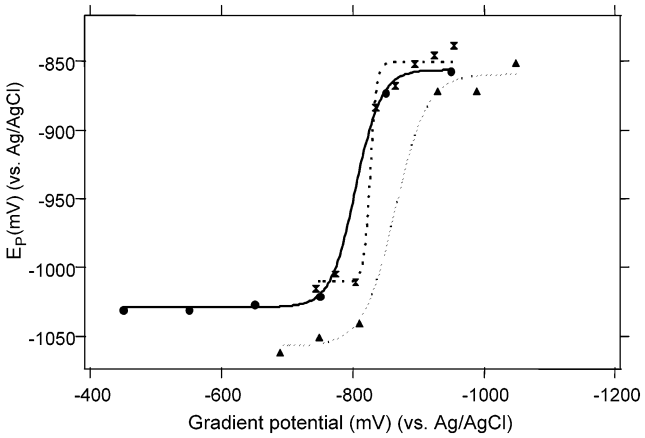

Figure 2. Stripping peak potentials as a function of gradient formation potential (position) for HDT one-component gradients formed from potential windows of different widths and center potentials: −300 to −1300 mV (solid); −600 to −1200 mV (dotted); −700 to −1000 mV (dashed).

$$E(x) = E_b + \frac{E_{max}}{1 + e^{(x_0 - x)/r}} \qquad (3)$$

where E_b is the base potential, E_{max} is the normalized maximum peak potential, x_0 is the inflection point of the slope region, and *r* is a spatial rate constant related to the slope. The width of the gradient, *W*, is determined from the full width at half-maximum of the derivative of the fit function, $dE(x)/dx$. The x_0 and *W* values can be interconverted between potential and physical space values using the width of the applied potential window, ΔV, and the total length of the film.

At spatial locations corresponding to local applied potentials, $V(x)$, more negative than ca. −1050 mV no desorption peak was observed, indicating that all the HDT had desorbed from the Au surface at positions where $V(x)$ is significantly more negative than the $E_{des}{}^0$ of a full HDT monolayer. In the transition region (−750 mV to −1050 mV; 27.5 to 17.5 mm in Figure 1), the HDT desorption waves are broad and not as well-defined as in a full HDT monolayer, consistent with a high degree of structural disorder for the HDT in this region. Incomplete HDT desorption in the transition region results in partial monolayers, which in turn produce broad electrochemical desorption peaks when profiled. For sample pieces where $V(x)$ is more positive than ca. −750 mV (ca. 35−50 mm along the position axis in Figure 1), the desorption peaks are well-defined, and the peak potentials are identical to those of the full HDT monolayer. Finally, the direction of the shift in E^0_{des} is exactly what is predicted by the Porter model. At gradient positions corresponding to the most negative gradient formation potentials, $V(x)$, the post-gradient stripping potential, E^0_{des}, is less negative, consistent with a less dense HDT layer.

Cyclic Voltammetry of Two-Component Gradients. In the biologically active gradients it is desirable to have two disparate functional groups, so that cellular adhesion may be laterally varied in a controlled fashion. Two-component gradients were prepared by immersing the one-component gradient samples in a solution of a second thiol for a short time, allowing the second thiol to adsorb in the exposed Au areas. For initial studies the HDT−MPA system was chosen, because the differing surface energies—HDT is terminated with a hydrophobic $-CH_3$ group and MPA is terminated with a hydrophilic −COOH moiety—facilitate characterization. Also the different chain lengths, C_{16} vs C_3, result in a large difference in $E_{des}{}^0$, −1040 mV and −950 mV for HDT and MPA SAMs, respectively, with HDT SAMs

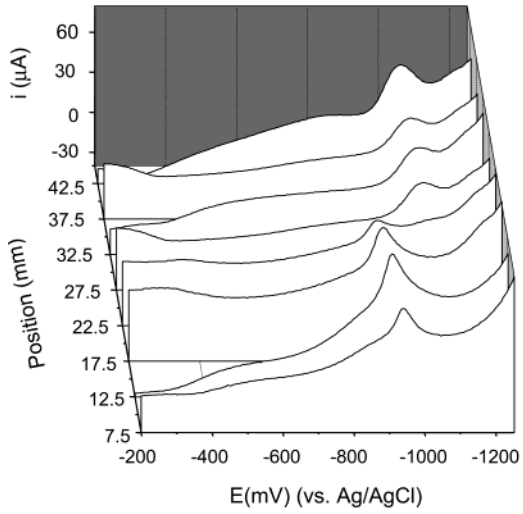

Figure 3. Spatially resolved CVs of a two-component HDT−MPA gradient formed with a 20 mV mm^{-1} in-plane potential gradient in 0.25 M KOH/MeOH. Position 7.5 mm corresponds to the MPA end, and 42.5 mm corresponds to the HDT end.

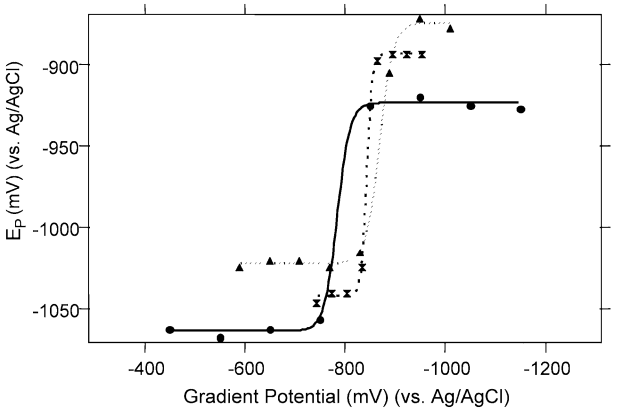

Figure 4. Stripping peak potentials with different applied potential windows as a function of gradient formation potential (position) for HDT−MPA two-component gradients formed from potential windows of different widths and center potentials: −300 to −1300 mV (solid); −500 to −1100 mV (dotted); −700 to −1000 mV (dashed).

yielding more negative desorption potential by ca. 100 mV due to the contributions of interchain interactions to the enthalpy of desorption. Thus, the in-plane composition variations in the transition region can be probed electrochemically.

Figure 3 shows the cyclic voltammograms of HDT/MPA counterpropagating gradients prepared with a 20 mV mm^{-1} in-plane potential gradient. The values of E_{des}^0 as a function of position (potential) are shown in Figure 4 demonstrating that the gradient centers remain relatively unchanged for applied potential windows widths ranging from $\Delta V = 300$ to 1000 mV. These observations are consistent with the linear potential gradient model implied in eq 1 which predicts that the gradient center will remain constant in potential space, even though it might move in physical space as the potential window is offset, as it is for the last of the 3 ΔV windows in Figure 4. Finally the transitions shown in Figure 4 for the two-component HDT/MPA gradient are noticeably sharper than those in Figure 2 for the one-component HDT gradient. This is expected, because MPA not only adsorbs in the exposed Au regions, it also exchanges with HDT, the latter reaction being especially facile in regions of low HDT surface population.

To test the hypothesis further gradients were also fabricated using different MPA adsorption times with a narrow applied

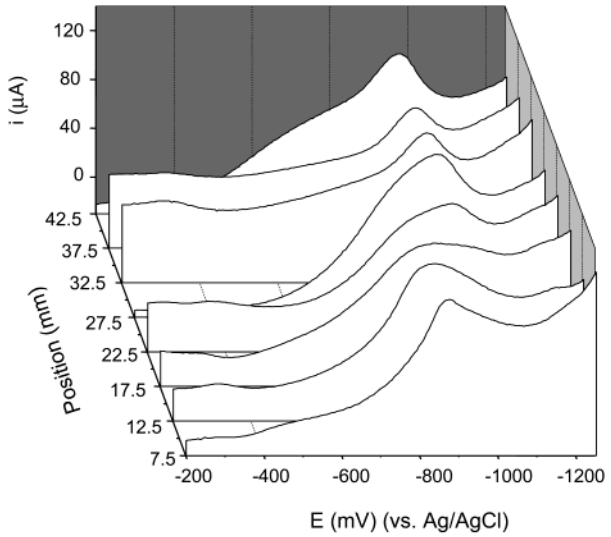

Figure 5. Spatially resolved CVs of a two-component HDT−MPA gradient formed from a gradient potential window of −700 to −1000 mV in 0.25 M KOH/MeOH, with the immersion of the initial HDT gradient in 1 mM MPA confined to 30 s. Position 7.5 mm corresponds to the MPA end, and 42.5 mm corresponds to the HDT end.

potential window (−700 to −1000mV) to accentuate the transition region. Figure 5 shows the effect of immersing the HDT gradient in MPA for shorter times (30 s). The desorption waves in the transition region are broader than those on the two pure-component ends of the gradient, and E_{des}^0 shifts from the MPA value to HDT value more slowly than in gradients prepared at longer MPA immersion times, cf. Figure 3, i.e. the slope in the transition region, $dE_{des}^0/dV(x) = 4.1$ mV mV^{-1}, is smaller than that for the same window in Figure 4, 8.6 mV mV^{-1}. At the shorter MPA adsorption times the HDT−MPA exchange process does not proceed as far, biasing the MPA population toward those molecules which just adsorb on the exposed Au area. Thus, the HDT and MPA in the transition region remain relatively disordered and less densely packed due to the short MPA adsorption time.

Taken together, the spatially resolved electrochemical stripping analysis experiments demonstrate that the reductive desorption behavior of alkanethiol SAMs faithfully follows the composition profiles of one- and two-component gradients of thiols. Furthermore, taking into account the factors which affect E_{des}^0, such as chain length and interchain interactions, allows both composition and molecular packing to be followed simultaneously, albeit at relatively poor spatial resolution, 0.5 cm.

Formation of Peptide−MUD Gradients. In the work described above two-component alkanethiol gradients with different terminal groups and chain lengths were formed and successfully mapped by electrochemical stripping analysis. To generate biologically active gradients, thiols terminated with surface ligands involving cell adhesion promoters, **1**, and inhibitors, MUD, were used. These terminal groups have been shown previously to be competent to control the attachment and morphology of endothelial cells and fibroblasts. Spatially resolved electrochemical stripping analysis has proven extremely useful in studying the composition and packing structure as a function of spatial position in alkanethiol gradients. However, when gradients were formed from peptide **1**, the large size of the molecules and the low surface coverage resulted in a small and broad desorption peak (not shown), thereby limiting the utility of stripping analysis. Fortunately Fourier transform infrared external reflection spectroscopy (FTIR-ERS) is well-

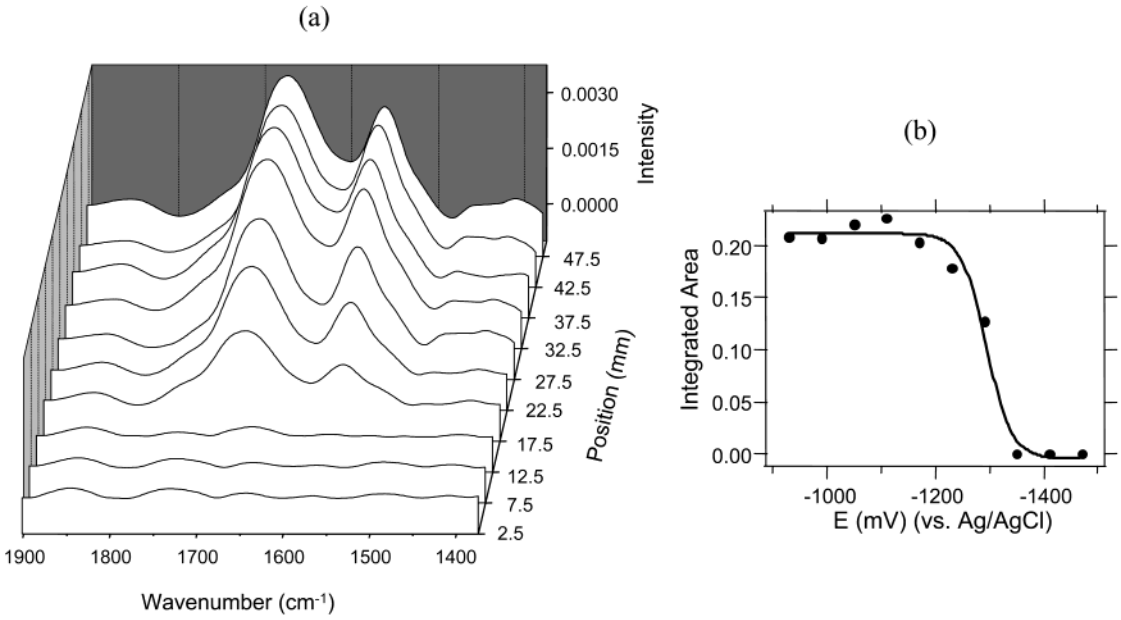

Figure 6. (a) FTIR-ERS spectra of a two-component MUD−**1** gradient produced with a gradient potential window of −900 to −1500 mV. Position 2.5 mm corresponds to the MUD end and 47.5 corresponds to the **1** end. (b) Integrated area of 1670 cm^{-1} band as a function of gradient potential (position).

TABLE 1. Gradient Center Values

gradient	potential range (mV)	potential window width (mV)	potential window center (mV)	gradient center (mV)	gradient width (mV)
MUD−**I**	−900 to −1500	600	−1200	−1296	81
MUD−**I**	−1000 to −1450	450	−1225	−1279	121
MUD−**I**	−1100 to −1400	300	−1250	−1266	125
MUD−20% **I**	−900 to −1500	600	−1200	−1243	42
MUD−20% **I**	−1050 to −1350	300	−1200	−1256	93

suited for the characterization of alkanethiol SAMs on Au[40] and is an especially good choice for direct chemical mapping of these gradients of MUD and peptide **1**, because the terminal functional groups give different infrared absorption spectra.

Figure 6 shows the FTIR-ERS spectra of two-component gradients of peptide **1** and MUD. Separate spectra of pure SAMs of **1** and MUD (not shown) illustrate that in the region of the amide I and amide II bands MUD exhibits only a weak, broad, undifferentiated absorption. Amide I and II bands were observed at 1670 cm^{-1} and 1550 cm^{-1}, respectively, on both pure SAM of peptide **1** and on MUD−**1** gradients at the peptide **1** end. No bands were observed from this spectral region in either the MUD SAM or the MUD end of a MUD−**1** gradient. Thus, these two bands can be used to probe the surface density of peptide **1**. The spectra as a function of position for the MUD−**1** gradient is shown in Figure 6(a). The transition region is characterized by fitting the intensity as a function of potential to eq 3, replacing potential terms, $E(x)$, E_b, and E_{max} with corresponding intensity terms $I(x)$, I_b, and I_{max}. The spatial resolution, ca. 5 mm, is comparable to that in the electrochemical stripping measurements above, but in the FTIR-ERS measurements it is limited by the need to use a large angle of incidence in order to achieve significant field amplitude at the interface. Obviously both amide I and II bands decrease in intensity as the local potential, $V(x)$, shifts negatively, i.e. toward the MUD end of the gradient (smaller position values in Figure 6(a)). Figure 6(b) shows a plot of the integrated area of the 1670 cm^{-1} band as a function of the gradient potential, $V(x)$. The transition region begins at a potential corresponding roughly to the stripping potential of peptide **1**, −1147 mV vs Ag/AgCl. Furthermore, the gradient center occurs negative of the stripping peak potential of **1**. This shift between the center potential of the gradient and the corresponding peak potential measured from CV is commonly observed and is expected, because the gradient formation process is static while cyclic voltammetry is inherently dynamic.

Compared with HDT/MPA gradients (Figure 4), the center of the MUD−**1** gradient transition region is more negative than the comparable region for HDT/MPA. Part of the explanation is undoubtedly that $E_{des}^0(\text{HDT}) = -1040$ mV is more positive than the $E_{des}^0(\mathbf{1}) = -1147$ mV by ca. 100 mV. The most likely reasons for the rest of the discrepancy in transition potential are kinetic in origin. Accounting for the difference between the dynamic nature of the cyclic voltammetry experiments from which E_{des}^0 values are obtained and the static nature of the spatially dependent stripping protocol, the observed difference could result from the difference in the electron-transfer rates between the alkanethiol HDT and the peptide-derivatized thiol **1**. This is a reasonable conjecture in light of previous observations that gradients of aromatic thiols need much longer stripping times than comparable alkanethiols.[31] This line of reasoning would posit a smaller desorption rate for **1** than HDT; thus requiring longer times and/or more negative potentials to desorb **1** from the surface.

The gradient formation characteristics are determined by the distribution of local electrochemical potential, $V(x)$, as given by eq 1. By varying the width of the potential window, ΔV, experimentally one can learn how the gradient formation characteristics change as the local potential, $V(x)$, is moved relative to the physical frame of the active region. When ΔV decreases while keeping the physical length of the gradient constant, the potential drop per unit length, dV/dx, decreases, meaning that the transition region occupies a larger physical

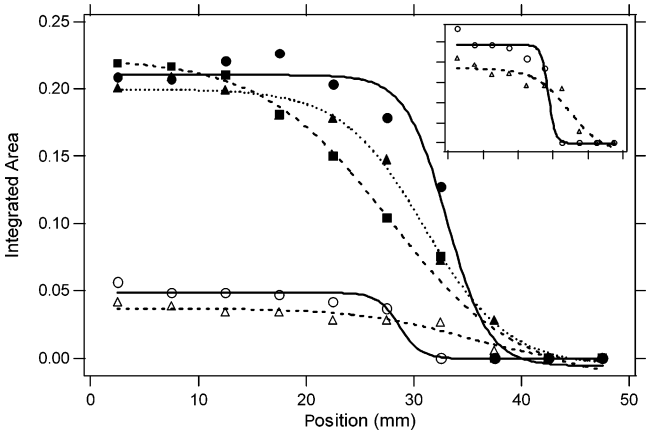

Figure 7. Integrated areas of the amide I band (1670 cm^{-1}) as a function of position for MUD−**1** gradients. Three gradients with larger saturation integrated areas were obtained from an initial 100% **1** SAM with the following gradient potential windows: −900 to −1500 mV (solid line, solid circles); −1000 to −1450 mV (dotted line, solid triangles); −1100 to −1400 mV (dashed line, solid squares). Two gradients with smaller saturation integrated areas were obtained from an initial 20% **1**−80% MUD SAM with the following gradient potential windows: −900 to −1500mV (solid line, open circles); −1050 to −1350mV (dashed line, open triangles). The inset shows the latter two mixed composition gradients at different scaling.

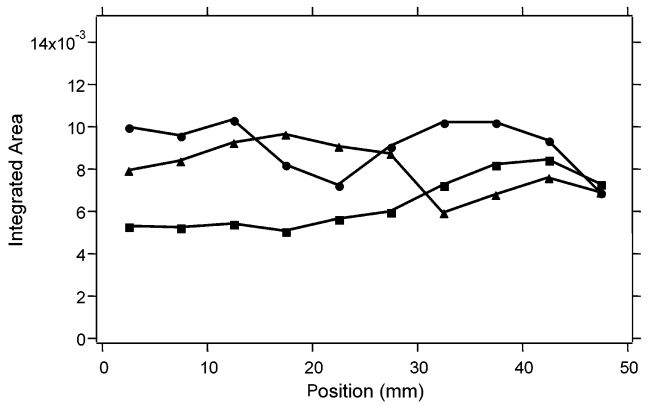

Figure 8. Integrated areas of the asymmetric methylene, ν_a (CH_2), band at 2921 cm^{-1} as a function of position for MUD−**1** gradients formed from different gradient potential windows: −900 to −1500 mV (solid circles); −1000 to −1450 mV (solid triangles); −1100 to −1400 mV (solid squares).

area of the film, although its width in potential space is unchanged. To test these hypotheses, experiments were performed in which ΔV was adjusted while characterizing the spatial properties of the **1**−MUD gradient by FTIR-ERS, as shown in Figure 7. It is apparent that in 0−100% MUD−**1** gradients the gradient center shifts to the left and the gradient becomes wider in physical space as the potential window width (ΔV) decreases. As expected the gradient center remains relatively constant in potential space as ΔV decreases from 600 to 300 mV (Table 1). These observations are consistent with the predictions of the quasi-linear potential gradient model, and importantly these gradients show $d\Gamma/dx$ values ranging from 0.15 mm^{-1} for the $\Delta V = 600$ mV window to 0.01 mm^{-1} for the 20% **1** gradient prepared with the $\Delta V = 300$ mV window. The ability to control the spatial rate of change of the integrin ligand density is a critical requirement for the use of these biomaterials in cell motility studies and assays.

The corresponding control experiment involves examining the asymmetric methylene stretching vibration, $\nu_{as}(CH_2)$ at ∼2921 cm^{-1}, which is observed from SAMs of either **1** or MUD, as a function of spatial position (Figure 8). Clearly the integrated area of $\nu_{as}(CH_2)$ does not change significantly. At first this is surprising, given the disparate numbers of $-CH_2-$ moieties in the two adsorbates. However, the surface selection rule states that only $-CH_2-$ groups in which the dynamic dipole, μ_{dip}, is oriented with a component perpendicular to the Au surface may couple effectively with the incident *p*-polarized electromagnetic field.[40] Thus, the greater number of $-CH_2-$ groups in **1** may be offset by a disordered structure in which a large fraction produce dynamic dipoles oriented preferentially parallel to the Au surface. Furthermore, this vibration overall is significantly weaker than the amide I vibration, so any differences as a function of position would be superimposed on a smaller total signal.

Conclusions

The electrochemical potential gradient method provides a convenient route to two-component counterpropagating composition gradients. Particularly useful is the ability to control the composition profile laterally. Because the two components can be chosen to have terminal solvent-accessible functional groups which vary widely, these surfaces can exert control over both chemical and physical properties of the solid−liquid interface. For example, formation of HDT/MPA gradients results in structures in which both surface energy ($-CH_3$ vs. $-COOH$ termination) and molecular packing (as measured through the local E_{des}^0) are anisotropic functions of lateral position. More complicated terminal moieties were explored through the formation of gradients of tetradecapeptide **1** in the presence of the protein adhesion-resistant MUD species. These gradients proved to be easily formed, and spatially resolved Fourier transform infrared external reflection spectroscopy was utilized to map functional group surface coverage of this gradient. The spatial intensity profiles were well described by the sigmoidal function in eq 3, from which the center potential and transition region width could be recovered. The gradient center was found to shift in physical space, but not in potential space, and the rate of compositional change, $d\Gamma/dx$, in the transition region was easily controlled when the width of the applied potential window, ΔV, was changed. These results are consistent with the quasi-linear potential gradient model in eq 1. The successful attainment of tunable composition gradients of a ligand for the important integrin superfamily of heterodimeric membrane receptors has important implications for the study of cellular motility and haptotactic behavior. We will report the results of these investigations separately.

Acknowledgment. This work was supported by grants from the National Institutes of Health (NIGMS GC10825, the Cell Migration Consortium) and the National Science Foundation (CHE 99-10236).

References and Notes

(1) Ingber, D. E. *Proc. Natl. Acad. Sci. U.S.A.* **1990**, *87*, 3579−3583.
(2) Boudreau, N.; Sympson, C. J.; Werb, Z.; Bissell, M. J. *Science* **1995**, *267*, 891−893.
(3) Basson, C. T.; Kocher, O.; Basson, M. D.; Asis, A.; Madri, J. A. *J. Cell. Phys.* **1992**, *153*, 118−128.
(4) Liu, S. Q.; Ito, Y.; Imanishi, Y. *J. Biomed. Mater. Res.* **1993**, *27*, 909−915.
(5) Massia, S. P.; Hubbell, J. A. *J. Biomed. Mater. Res.* **1991**, *25*, 223−242.
(6) Kang, I. K.; Kwon, B. K.; Lee, J. H.; Lee, H. B. *Biomaterials* **1993**, *14*, 787−792.
(7) Berggren, K. K.; Bard, A.; Wilbur, J. L.; Gillaspy, J. D.; Helg, A. G.; McClelland, J. J.; Rolston, S. L.; Phillips, W. D.; Prentiss, M.; Whitesides, G. M. *Science* **1995**, *269*, 1255−1257.

(8) Singhvi, R.; Kumar, A.; Lopez, G. P.; Stephanopoulos, G. N.; Wang, D. I. C.; Whitesides, G. M.; Ingber, D. E. *Science* **1994**, *264*, 696−698.
(9) Prime, K. L.; Whitesides, G. M. *Science* **1991**, *252*, 1164−1167.
(10) Wu, P.; Hoying, J. B.; Williams, S. K.; Kozikowski, B. A.; Lauffenburger, D. A. *Ann. Biomed. Eng.* **1994**, *22*, 144−152.
(11) Dimilla, P. A.; Stone, J. A.; Quinn, J. A.; Albelda, S. M.; Lauffenburger, D. A. *J. Cell Biol.* **1993**, *122*, 729−737.
(12) Goodman, S. L.; Risse, G.; Vondermark, K. *J. Cell Biol.* **1989**, *109*, 799−809.
(13) Huttenlocher, A.; Ginsberg, M. H.; Horwitz, A. F. *J. Cell Biol.* **1996**, *134*, 1551−1562.
(14) Maheshwari, G.; Wells, A.; Griffith, L. G.; Lauffenburger, D. A. *Biophys. J.* **1999**, *76*, 2814−2823.
(15) Palecek, S. P.; Loftus, J. C.; Ginsberg, M. H.; Lauffenburger, D. A.; Horwitz, A. F. *Nature* **1997**, *385*, 537−540.
(16) Ruoslahti, E.; Pierschbacher, M. D. *Science* **1987**, *238*, 491−497.
(17) Roberts, C.; Chen, C. S.; Mrksich, M.; Martichonok, V.; Ingber, D. E.; Whitesides, G. M. *J. Am. Chem. Soc.* **1998**, *120*, 6548−6555.
(18) Houseman, B. T.; Mrksich, M. *Biomaterials* **2001**, *22*, 943−955.
(19) Maheshwari, G.; Brown, G.; Lauffenburger, D. A.; Wells, A.; Griffith, L. G. *J. Cell Sci.* **2000**, *113*, 1677−1686.
(20) Wilkinson, P. C. *J. Immun. Methods* **1998**, *216*, 139−153.
(21) Herbert, C. B.; McLernon, T. L.; Hypolite, C. L.; Adams, D. N.; Pikus, L.; Huang, C. C.; Fields, G. B.; Letourneau, P. C.; Distefano, M. D.; Hu, W. S. *Chem. Biol.* **1997**, *4*, 731−737.
(22) Liedberg, B.; Tengvall, P. *Langmuir* **1995**, *11*, 3821−3827.
(23) Liedberg, B.; Wirde, M.; Tao, Y. T.; Tengvall, P.; Gelius, U. *Langmuir* **1997**, *13*, 5329−5334.
(24) Hypolite, C. L.; McLernon, T. L.; Adams, D. N.; Chapman, K. E.; Herbert, C. B.; Huang, C. C.; Distefano, M. D.; Hu, W. S. *Bioconjugate Chem.* **1997**, *8*, 658−663.
(25) Jeon, N. L.; Dertinger, S. K. W.; Chiu, D. T.; Choi, I. S.; Stroock, A. D.; Whitesides, G. M. *Langmuir* **2000**, *16*, 8311−8316.
(26) Dertinger, S. K. W.; Jiang, X. Y.; Li, Z. Y.; Murthy, V. N.; Whitesides, G. M. *Proc. Natl. Acad. Sci. U.S.A.* **2002**, *99*, 12542−12547.
(27) Terrill, R. H.; Balss, K. M.; Zhang, Y. M.; Bohn, P. W. *J. Am. Chem. Soc.* **2000**, *122*, 988−989.
(28) Balss, K. M.; Coleman, B. D.; Lansford, C. H.; Haasch, R. T.; Bohn, P. W. *J. Phys. Chem. B* **2001**, *105*, 8970−8978.
(29) Plummer, S. T.; Bohn, P. W. *Langmuir* **2002**, *18*, 4142−4149.
(30) Balss, K. M.; Fried, G. A.; Bohn, P. W. *J. Electrochem. Soc.* **2002**, *149*, C450−C455.
(31) Balss, K. M.; Kuo, T. C.; Bohn, P. W. *J. Phys. Chem. B* **2003**, *107*, 994−1000.
(32) Walczak, M. M.; Popenoe, D. D.; Deinhammer, R. S.; Lamp, B. D.; Chung, C. K.; Porter, M. D. *Langmuir* **1991**, *7*, 2687−2693.
(33) Viana, A. S.; Kalaji, M.; Abrantes, L. M. *Electrochim. Acta* **2002**, *47*, 1587−1594.
(34) Palegrosdemange, C.; Simon, E. S.; Prime, K. L.; Whitesides, G. M. *J. Am. Chem. Soc.* **1991**, *113*, 12−20.
(35) Pertsin, A. J.; Grunze, M.; Garbuzova, I. A. *J. Phys. Chem. B* **1998**, *102*, 4918−4926.
(36) Prime, K. L.; Whitesides, G. M. *J. Am. Chem. Soc.* **1993**, *115*, 10714−10721.
(37) Widrig, C. A.; Chung, C.; Porter, M. D. *J. Electroanal. Chem.* **1991**, *310*, 335−359.
(38) Weisshaar, D. E.; Walczak, M. M.; Porter, M. D. *Langmuir* **1993**, *9*, 323−329.
(39) Zhong, C. J.; Porter, M. D. *J. Am. Chem. Soc.* **1994**, *116*, 11616−11617.
(40) Terrill, R. H.; Tanzer, T. A.; Bohn, P. W. *Langmuir* **1998**, *14*, 845−854.